

# Histogram Analysis of the Microvasculature of Intracerebral Human and Murine Glioma Xenografts

Nathalie Just<sup>1,2\*</sup>

The purpose of this study is to examine the usefulness of histogram analysis combined with vessel size index (VSI) magnetic resonance imaging for the specific characterization of brain tumor microvasculature in a panel of six volume-matched glioma xenografts. Using a simple descriptive histogram analysis, significant differences of the mean tumoral VSI ( $P = 0.0035$  for 9L,  $P = 0.008$  for glioma mix,  $P = 0.05$  for C6), the 75th VSI percentile ( $P = 0.003$ – $0.075$ ) as well as the 25th and median blood volume (BV) percentiles were found in murine gliomas compared to their contralateral healthy brain. Using a segmented histogram analysis, dilatation of already existing vessels in murine gliomas and development of new small caliber vessels in human glioblastomas were suggested. Most gliomas showed a higher proportion of pixels with BV below 1% (glioma mix [21% vs 1%], Glioblastoma 2 (GBM2) [9% vs 3.7%]) and a smaller proportion of pixels with BV in the range 1.7–6.3% (65 vs 90% for glioma mix, 80 vs 85% in GBM2) relative to their contralateral part. In glioblastomas, VSI and BV distributions were similar to normal brain distributions and in agreement with immunohistochemical findings. The histogram analysis of VSI and BV heterogeneity in experimental brain tumors allowed detection of microregional differences in gliomas from different origins. *Magn Reson Med* 65:778–789, 2011. ©2010 Wiley-Liss, Inc.

**Key words:** gliomas; histogram; segmented; vessel size index

## INTRODUCTION

To deal with the heterogeneity of most tumors, voxel-by-voxel analyzes are nowadays preferred and allow visual delineation of specific areas in tumors pre- and post-treatment. Histogram analysis of various parameters such as permeability ( $K^{trans}$ ), blood volumes (BVs), blood flow are thus possible (1,2). Nevertheless, obtaining and comparing quantitative data from histograms remains difficult and time-consuming. Quantitative voxel-by-voxel values are very often pooled to calculate mean and median values that are not always significantly sensitive to treatment effects. There is therefore a need to define user-friendly methods to analyze histogram data in cancer magnetic resonance imaging (MRI) studies. It is also important to investigate the true value of using histogram analysis.

High grade gliomas are particularly aggressive tumors characterized by their high angiogenic levels (3,4). The

vascular endothelial growth pathway appears particularly important and has been a prominent therapeutic target in cancer treatment of gliomas. Moreover, these brain tumors are also characterized by their high heterogeneity from one patient to another but also from one area within the tumor to another. The identification of biomarkers to predict response or resistance to treatment and to monitor angiogenic effects is important. This will be possible if the neovasculature of gliomas can be accurately described. The vessel size index (VSI) MRI technique allows to investigate brain tumor microvasculature using high molecular superparamagnetic contrast agents in rats (5) and gadolinium chelates in humans (6). The mean vessel caliber estimation relies on the simultaneous measurement of  $\Delta R_2^*$  and  $\Delta R_2$  after administration of contrast agent. Previous animal studies on normal brain and C6 gliomas showed the usefulness of this method for the characterization of the tumor neovascularization: highly vascularized regions corresponded to high BV regions, necrotic regions corresponded to low BV regions and viable tumor regions showed large vessel sizes with lower BV values compared to contralateral healthy brain areas (7). All these results were well correlated to histological measurements. In humans, the VSI MR technique showed an added value for brain histopathology evaluation. The VSI MRI technique could potentially be described as a noninvasive “histological” method.

The purpose of the present study was to investigate and compare the vascularization of a panel of six aggressive brain tumors using histogram analysis of VSI and BV maps. In addition to the usual descriptive histogram analysis, a “segmentation” of each tumor type histogram was performed allowing further characterization of the microvasculature of our six gliomas.

## MATERIALS AND METHODS

### Cell Culture

All the cell suspensions were obtained from in vitro cells grown as monolayers at 37°C in a humidified atmosphere. RPMI640 was used as the culture medium. The cells were adherent to plastic flasks. After two washes, the cells were put back in RPMI640 medium at the cell density of  $2 \times 10^7$  cells/mL. In their exponential growth phase, the tumor cells were detached from the culture flask by a 2-minute treatment with trypsin-versene (Biowhittaker, Ref BE14-603E, Batch No 7SB0009/20R) and used for experimental purposes.

### Murine Glioma Cell Lines

The GLM (Glioma Mix) cell line was obtained from an intracerebral mixed glioma after injection of *N*-ethyl-*N*-nitrosourea (ENU) in a BDIX rat. The 9L cell line was

<sup>1</sup>Laboratory for functional and metabolic imaging (LIFMET), EPFL, UNIL, Centre d'Imagerie Biomédicale, Lausanne, Switzerland.

<sup>2</sup>Department of Radiology, UNIL, Centre d'Imagerie Biomédicale, Lausanne, Switzerland.

\*Correspondence to: Nathalie Just, Ph.D., LIFMET CIBM Centre d'Imagerie BioMedicale, EPFL, CHF1626 (Bâtiment CH), Lausanne CH-1015, Switzerland. E-mail: nathalie.just@epfl.ch

Received 6 January 2010; revised 26 August 2010; accepted 14 September 2010.

DOI 10.1002/mrm.22675

Published online 3 November 2010 in Wiley Online Library (wileyonlinelibrary.com).

© 2010 Wiley-Liss, Inc.

Table 1  
MRI and Survival Studies

Glioma	Group	Rat Nb	T2-w MRI	Diffusion, VSI	Mean Survival $\pm$ SD
9L	MRI	8	D11	D12	
-	Surv	5			15.0 $\pm$ 1.0
GLM	MRI	6	D9	D10	
-	Surv	3			13.3 $\pm$ 0.6
C6	MRI	8	D17	D18	
-	Surv	5			28.3 $\pm$ 6.8
U87-MG	MRI	6	D19	D20	
-	Surv	4			26.5 $\pm$ 1.9
GBM1	MRI	5	D48	D49,D53	
-	Surv	3			66.3 $\pm$ 5.0
GBM2	MRI	5	D23	D24,D28	
-	Surv	5			33.4 $\pm$ 1.9

For each tumor cell line the numbers of rats attributed to MRI and survival studies are given. Days post-tumor implantation when  $T_2$ -weighted imaging diffusion and VSI MR imaging were performed are given together with the mean survival time for each group of rats.

obtained from a chemo-induced gliosarcoma after ingestion of *N*-methyl-*N*-nitrosourea (MNU) in the Fisher 344 rat. The C6 cell line was obtained from a chemo-induced astrocytoma after injection of *N*-methyl-*N*-nitrosourea (MNU) in the Wistar rat.

#### Human Glioma Cell Lines

The GBM1 and Glioblastoma 2 (GBM2) cell lines were respectively obtained from a TG-8 and a SNB-19 human glioblastomas (Institut Curie, Paris, France) grown subcutaneously in nude rats. U87-MG grade III astrocytoma human cell lines were obtained from the American type culture collection (ATCC, Rockville, MD).

#### Xenograft Tumor Studies

One hundred thousand cancer cells were injected stereotactically in the right caudate nucleus at a depth of 4.5 mm in twenty male rats per cancer cell line (Wistar rats for C6 cancer cells, BDIX rats for GLM cancer cells, Fisher rats for 9L cancer cells and Nude rats for GBM2, GBM1, and U87-MG cancer cells). Animal care and all the experiments performed on the animals conformed to the guidelines of the Animal Experimental Committee of the Institution.

Ten rats per cancer cell line were kept for survival studies and ten rats were used for MRI investigations as described in Table 1.

#### Magnetic Resonance Imaging

All the imaging experiments were performed in a 2.35T horizontal bore magnet interfaced with a SMIS console. Each MRI session started with the anesthesia of a rat with a mixture of isoflurane in air and oxygen (30/70). After catheterization in one of the tail veins, the rat was placed in the magnet under continuous isoflurane anesthesia. The rat body temperature was monitored by a rectal probe and maintained at a physiological temperature ( $37^\circ\text{C} \pm 1^\circ\text{C}$ ) by a heating pad placed under the abdomen. A surface coil for reception and a volume coil for transmission (Rapid Biomedical, Germany) were used.

Multislice spin echo  $T_2$ -weighted MRI (TR/TE = 2000/80 ms; FOV =  $30 \times 30$  mm; matrix =  $128 \times 64$ ; 15 axial slices; slice thickness = 1 mm) was performed for mor-

phological evaluation of brain tumors and tumor volume calculation. Several MR  $T_2$ -weighted measurements were organized during each glioma development.

Apparent diffusion coefficient (ADC), VSI, and BV values were determined when MR measured tumor volumes were  $61 \pm 12$  mm<sup>3</sup>. GBM1 and GBM2 were examined on two occasions at 4 days interval.

A Stejskal-Tanner diffusion-weighted MRI sequence was used for ADC mapping (TR/TE = 2000/80 ms; FOV = 30 mm; matrix =  $128 \times 64$ ; 15 axial slices; slice thickness = 1 mm). A diffusion gradient with a  $b$  value of 500s/mm<sup>2</sup> was applied along the X, Y, and Z directions successively.

Finally, a multi gradient echo spin echo for VSI and BV evaluation was applied (TR = 6000 ms; FOV = 30 mm; matrix =  $256 \times 64$ ; 15 axial slices; slice thickness = 1 mm). Four minutes after injection of the intravascular contrast agent (Sinerem, Guerbet, France, 200  $\mu\text{mol}$  Fe/kg), the multigradient echo-spin echo sequence was repeated. The total acquisition time for one rat was 2 hours.

#### Data Analysis

All the images were transferred to a SUN workstation to be processed under IDL 5.1 (Interactive Data Language; RSI; Boulder; Colorado). Regions of interest (ROIs) encompassing the tumor were drawn manually over three slices at the center of each tumor for each model. In each case, a contralateral region of interest of equivalent surface was also drawn.

VSI maps were derived from water ADC,  $\Delta R_2$  and  $\Delta R_2^*$  maps [see Eqs. 1 and 2] while volume maps (BV) were proportional to  $\Delta R_2^*$  maps [see Eq. 3] along the lines described by Troprès et al. (5). The pixels corresponding to a BV exceeding 17% were excluded from the computation as well as the VSI values exceeding 100  $\mu\text{m}$  (5).

$$\text{VSI}(\mu\text{m}) = 1.77 * \left( \frac{\gamma \Delta \chi B_0}{\text{ADC}} \right)^{1/3} \frac{\Delta R_2}{\Delta R_2^*} \quad [1]$$

with

$$D_{kk} = -\frac{1}{b} \ln \left( \frac{S(b)}{S(0)} \right); \text{Trace}(D) = D_{xx} + D_{yy} + D_{zz}; \quad \text{ADC} = \frac{1}{3} \text{Trace}(D) \quad [2]$$

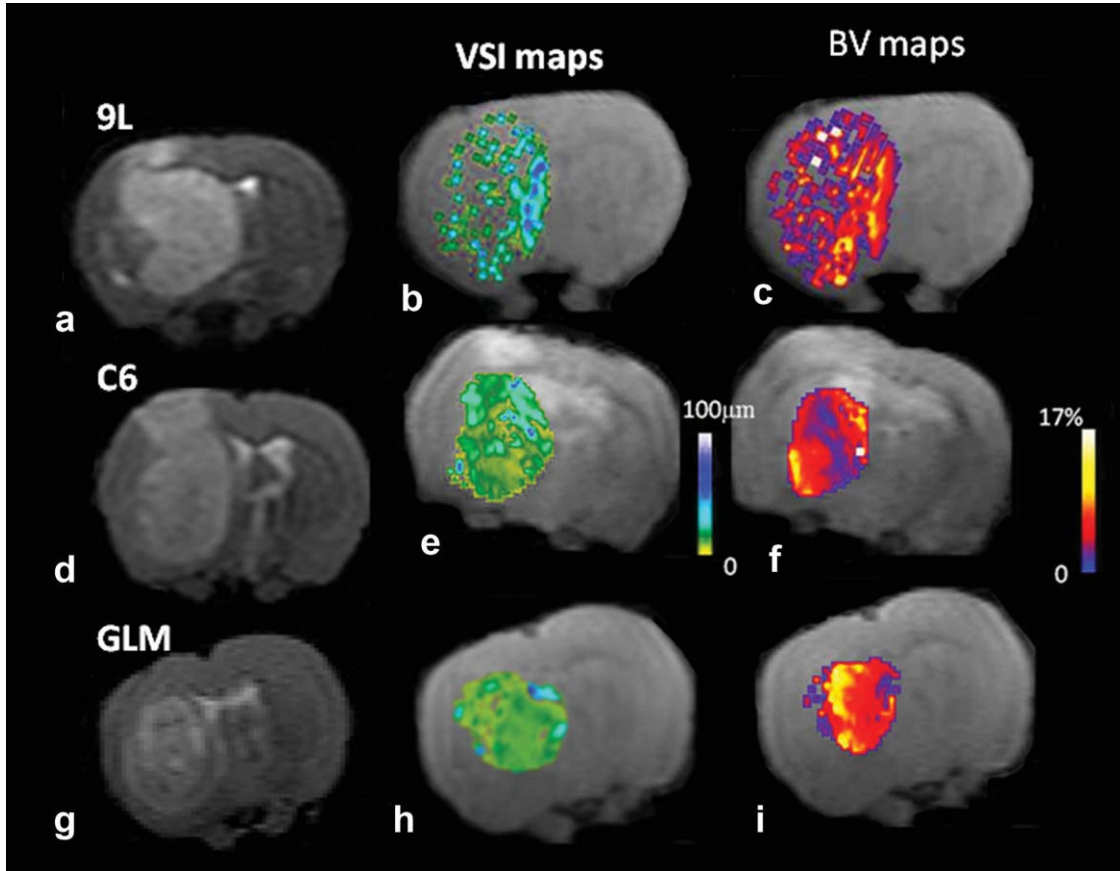


FIG. 1. Anatomical, VSI and BV maps of brain tumors from murine origin:  $T_2$ -weighted spin-echo anatomical images (A-D-G) (TR/TE = 2000/80 ms; FOV =  $30 \times 30$  mm; matrix =  $128 \times 64$ ; 15 axial slices; slice thickness = 1 mm), false color VSI pixel by pixel maps (B-E-H) overlaid over multigradient echo-spin echo images and false color BV pixel by pixel maps (C-F-I) overlaid over multigradient echo-spin echo images successively for 9L a murine gliosarcoma, C6 a murine astrocytoma and GLM a mixed glioma. The color bar is represented on the right.

$$BV(\%) = \frac{3}{4\pi} \frac{\Delta R_2^*}{\gamma \Delta \chi B_0} \quad [3]$$

The ADC was averaged over three slices within tumors and within the healthy contralateral part of the rat brain. Regions of interest (ROIs) encompassing the whole tumor were drawn manually. ROIs in the contralateral brain were symmetrically drawn and of identical sizes. The averaged ADC value was used for VSI calculation. For each model, five to six tumors were analyzed. Pixel by pixel VSI and  $\Delta R_2^*$  false color maps were obtained for each of the 3 slices taken into account.

## Histogram Analysis

### Simple Histogram Analysis

To investigate the distribution of VSI and BV over each tumor and its contralateral area, histogram distributions were obtained for each of the three tumor slices and the contralateral areas. One single histogram encompassing the data from these three slices was obtained. To eliminate the influence of tumor volume, VSI and BV pixel values were normalized to the total number of pixels contained in the ROI.

Using XLSTAT (Microsoft Excel, Addinsoft), conventional descriptive measures: Mean, Median 25th percen-

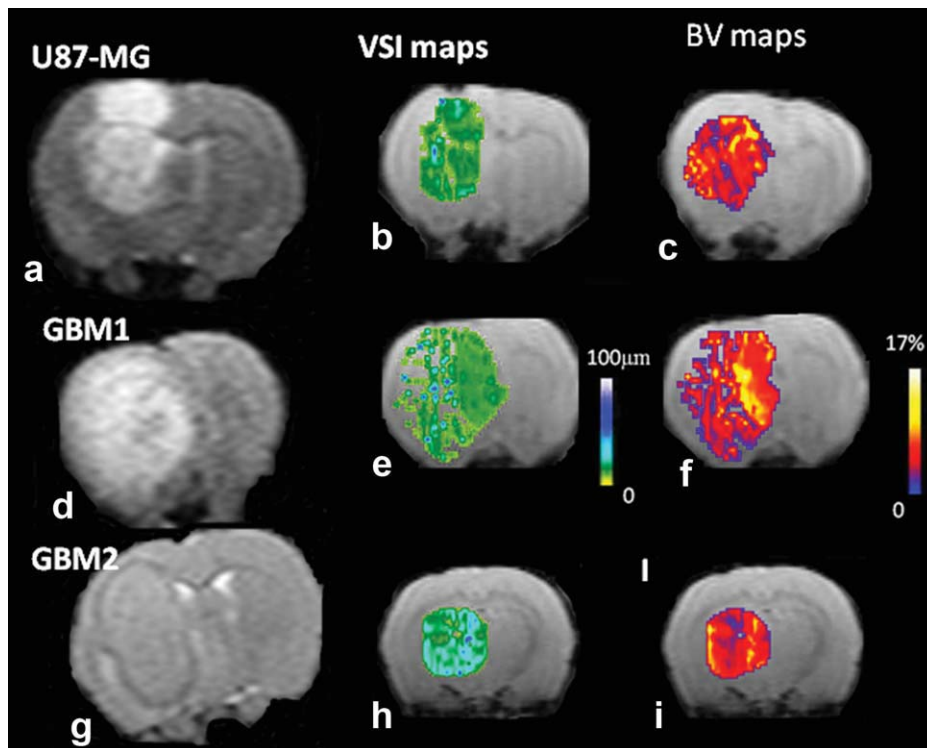
tile, 75th percentile, skewness and kurtosis of the VSI and  $\Delta R_2^*$  distributions were obtained for each tumor type. The group average (mean  $\pm$  SD) was calculated for each tumor type and their contralateral healthy part and the significance of the differences between tumor tissue and healthy tissue were evaluated using a two-sided paired t-test. A  $P < 0.05$  was considered significant.

### Histogram Segmentation

For each glioma model and contralateral area, proportions of VSI pixel values were divided into 4 categories corresponding to 2–4  $\mu\text{m}$ , 4–6  $\mu\text{m}$ , 6–10  $\mu\text{m}$  and values above 10  $\mu\text{m}$ . The  $\Delta R_2^*$  pixel values were divided into 5 categories 10–15  $\text{s}^{-1}$ , 15–25  $\text{s}^{-1}$ , 25–45  $\text{s}^{-1}$ , 45–95  $\text{s}^{-1}$  and over 95  $\text{s}^{-1}$  corresponding to the 5 categories 0–1%, 1–1.7%, 1.7–3%, 3–6.5% and over 6.5% using Eq. 3 with  $\Delta \chi = 1.57 \times 10^{-7}$  (5). For each category of VSI and BV mean  $\pm$  SEM was calculated for each tumor type and their contralateral healthy part and the significance of the differences between tumor tissue and healthy tissue were evaluated using a two-sided paired t-test. A  $P < 0.05$  was considered significant.

*Immunohistochemical staining and histology.* All the rats were injected intravenously via the tail vein with a PBS solution (phosphate buffered saline, pH = 7.4) containing

FIG. 2. Anatomical, VSI and BV maps of brain tumors from human origin:  $T_2$ -weighted spin-echo anatomical images (A-D-G) (TR/TE = 2000/80 ms; FOV = 30 × 30 mm; matrix = 128 × 64; 15 axial slices; slice thickness = 1 mm), false color VSI pixel by pixel maps (B-E-H) overlaid over multigradient echo-spin echo images and false color BV pixel by pixel maps (C-F-I) overlaid over multigradient echo-spin echo images successively for U87-MG human astrocytoma, GBM1 and GBM2 two glioblastomas from human origin. The color bar is represented on the right. [Color figure can be viewed in the online issue, which is available at [wileyonlinelibrary.com](http://wileyonlinelibrary.com).]



15mg/kg of the perfusion marker Hoechst 33342 (Sigma Aldrich, St. Louis, MO). One minute after the injection, animals were killed. Tumors were quickly removed, frozen and stored in liquid nitrogen. For the analysis, four sections of 5 μm thickness at the center of each tumor and four other sections at the periphery were made using a cryotome. The sections were incubated with an antibody against the basal lamina component collagen type IV to delineate functional and non perfused vasculature in tumors and their healthy contralateral part. Qualitative image analysis only was performed using a fluorescence microscope to examine the vasculature of the tumors on three sections per tumor (8). Haematoxylin and eosin stained sections were also made for histological examination.

**RESULTS**

**Anatomical Characteristics of Xenografted Gliomas**

Typical examples of  $T_2$ -weighted images are shown in Fig. 1 for the murine gliomas (Fig. 1A-D-G) and in Fig. 2 for the human gliomas (Fig. 2A-D-G).

The periphery of GLM gliomas (Fig. 1G) demonstrated a characteristic hypointensity on  $T_2$ -weighted SE images corresponding to a cystic periphery according to histological findings. GBM2 gliomas (Fig. 2G) were all isointense on  $T_2$ -weighted images relative to the normal brain. On the contrary, 9L, C6, GBM1 and U87-MG tumors were hyperintense on  $T_2$ -weighted MR images.

**VSI and Cerebral BV**

*Mean and Median VSI and Cerebral BV Based on Whole Volume ROI Analysis*

Mean ADC values in tumors and their contralateral side are reported in Table 2.

In the contralateral brain, the mean VSI was  $3.63 \pm 0.95 \mu\text{m}$ . Wistar rats bearing C6 tumors had the highest mean VSI value ( $5.1 \pm 1.5 \mu\text{m}$ ) in the healthy contralateral brain, whereas BDIX rats bearing GLM tumors had the lowest mean VSI ( $3.38 \pm 1.7 \mu\text{m}$ ).

The bigger vessel size indices were found in the gliomas of murine origin where the mean VSI ranged between  $4.46 \pm 0.7$  and  $6.92 \pm 2 \mu\text{m}$ . 9L, C6 and GLM gliomas all showed significantly higher VSI values relative to their contralateral healthy part (Table 3). These gliomas also presented the largest differences in VSI with their contralateral areas, whereas in the gliomas of human origin, mean VSI values were almost similar to the mean VSI values in the contralateral brain (Fig. 3A).

Mean BV (Fig. 3B) values were higher in the contralateral brain than in U87-MG, C6 and GBM1 tumors but not statistically different (paired t-test  $P > 0.05$ ) except for C6 (paired t-test,  $P = 0.009$ ). In the rats bearing human gliomas, mean BV are all above 3% in both the gliomas and the contralateral brain areas. The difference between the glioma and its contralateral area was in general higher for murine gliomas. Figure 3C,D show median

Table 2  
Mean ADC ± Standard Deviation (SD) of Gliomas and Contralateral Area (Contra) Used for the VSI-BV Analysis

Glioma	ADC ( $\mu\text{m}^2\text{s}^{-1}$ )	SD	ADC Contra ( $\mu\text{m}^2\text{s}^{-1}$ )	SD
9L	1417	183	958	220
C6	1293	62	898	72
GLM	1480	111	912	78
GBM2	968	56	882	109
GBM1	1086	66	801	22
U87-MG	1429	256	1035	232

Table 3  
VSI Statistics

Gliomas	C6	GLM	9L	U87-MG	GBM1	GBM2
Mean	0.052	0.008	0.0035	0.57	0.87	0.32
Skewness	0.34	$P < 0.0001$	0.25	0.1	0.46	0.92
Kurtosis	0.37	0.005	0.26	0.25	0.36	0.86
25th percentile	0.76	0.62	0.28	0.16	0.16	0.4
Median	0.13	0.93	0.13	0.7	0.81	0.12
75th percentile	0.075	0.003	0.061	0.26	0.4	0.84

Student paired t-tests were performed to compare the Mean VSI, histogram skewness, kurtosis, 25th and 75th percentiles and median values between each brain tumor cell line and their contralateral healthy part. *P*-values are reported that were considered significant for  $P < 0.05$ . The significant *P*-values are highlighted (gray cells).

VSI and BV comparisons respectively (mean median of each group of tumors  $\pm$  SEM) between each glioma line and contralateral healthy tissue. The statistical analysis is presented in Tables 3 and 4. Median VSIs were higher in gliomas than their contralateral side but no significant difference was found. Median BV showed a significant difference for C6 gliomas (t-test,  $P = 0.005$ ).

Typical examples of VSI and BV maps over each type are also displayed in Figs. 1 and 2. VSI maps are represented on the second columns (Figs. 1B-E-H and 2B-E-H) and BV maps are represented in the last columns (Figs. 1C-F-I and 2C-F-I).

In the parametric pixel by pixel maps, blue values represent the lowest values, whereas yellow-white pixel values are the highest. All the tumors presented large

regions with small vessel sizes. 9L (Fig. 1B,C) and GBM1 (Fig. 2E,F) tumors showed regions where VSI and/or BV failed to be mapped due either to model limits being reached in these areas or to fit failures concerning  $R_2^*$  mapping or to necrosis or lack of vessel functionality. These problems were often encountered in 9L, U87-MG and GBM1 gliomas on their second scanning session. C6 gliomas demonstrated increased vessel calibers over wider tumor regions. Only a few pixels with high vessel calibers ( $> 40 \mu\text{m}$ ) were mapped particularly in the gliomas of human origin. GLM gliomas reproducibly showed characteristic patches of yellow-white pixels. BV maps were more homogeneous over the tumors than the VSI maps. A large percentage of red pixels with BVs in the range 2–6% were always represented.

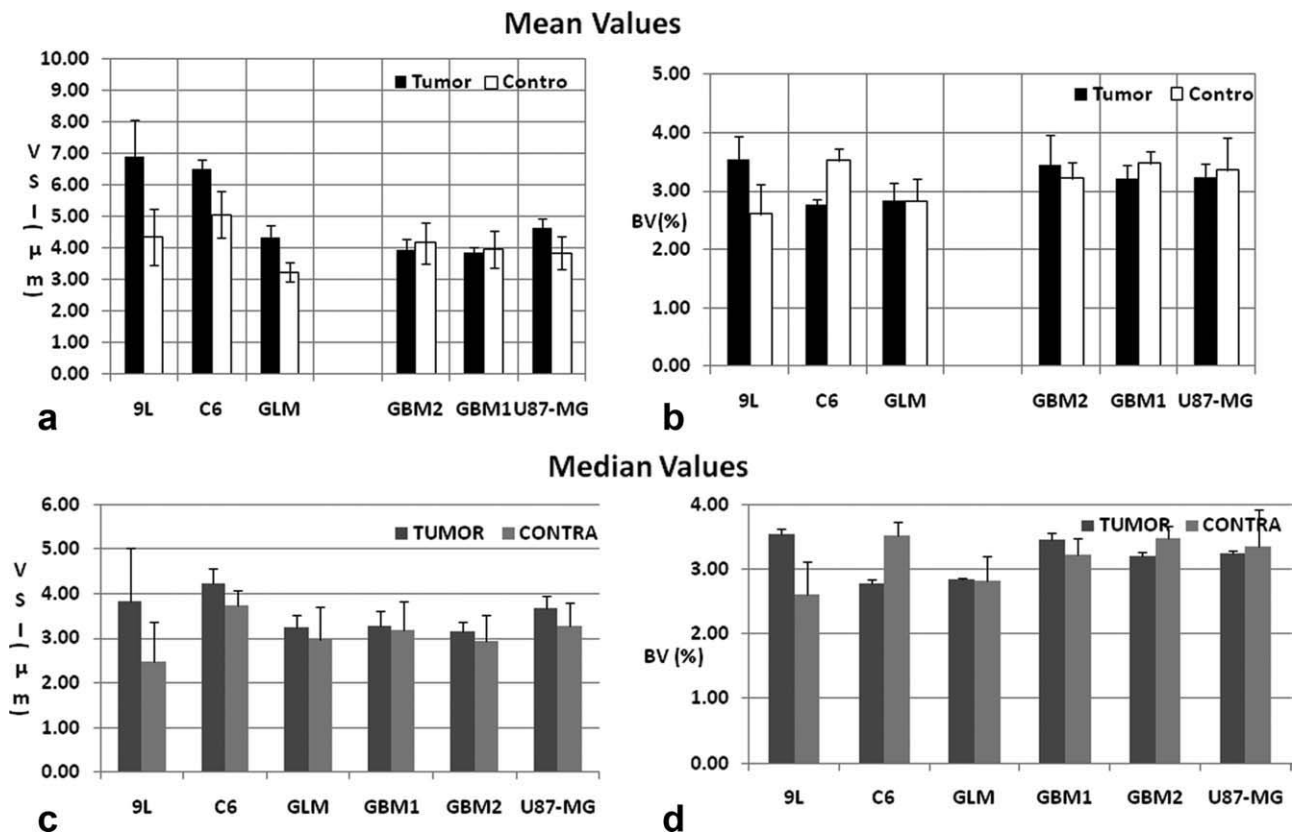


FIG. 3. Comparison of mean and median tumor VSI (A-C) and mean and median tumor BV values (blood volume) (B-D) (Mean  $\pm$  SEM). Each tumor type is compared to its contralateral part. Murine tumors are presented on the left part of each graph. Only murine brain tumors presented significant differences compared their corresponding contralateral part. In particular mean tumor VSI values were significantly higher. Mean and median BV values were significantly smaller for C6 only.

Table 4  
Blood Volume Statistics

Gliomas	C6	GLM	9L	U87-MG	GBM1	GBM2
Mean	0.009	0.4	0.16	0.63	0.34	0.35
Skewness	0.63	0.18	0.009	0.28	0.09	0.18
Kurtosis	0.36	0.081	0.016	0.1	0.36	0.8
25th percentile	0.04	0.48	0.6	0.06	0.98	0.32
Median	0.005	0.97	0.24	0.32	0.55	0.19
75th percentile	0.06	0.023	0.1	0.4	0.12	0.1

Student paired t-tests were performed to compare the Mean  $\Delta R_2^*$ , histogram skewness, kurtosis, 25th and 75th percentiles and median values between each brain tumor cell line and their contralateral healthy part. *P*-values are reported that were considered significant for  $P < 0.05$ . The significant *P*-values are highlighted (gray cells).

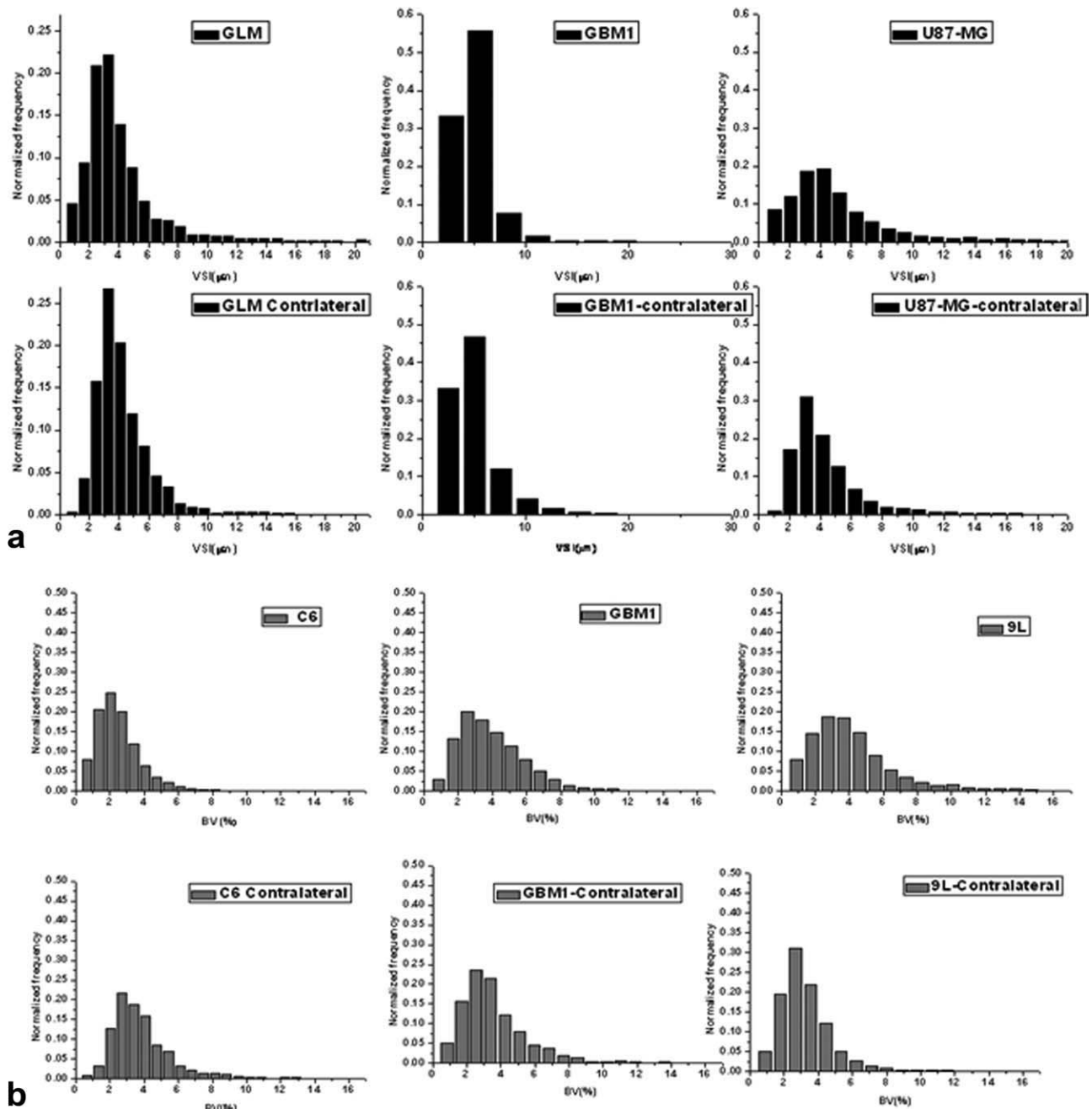


FIG. 4. Simple histogram analysis: Comparison of Histogram distributions in brain tumors and their contralateral healthy part. (A) for VSI in GBM1, GLM, and U87-MG (B) for BV in C6, GBM1, and 9L.

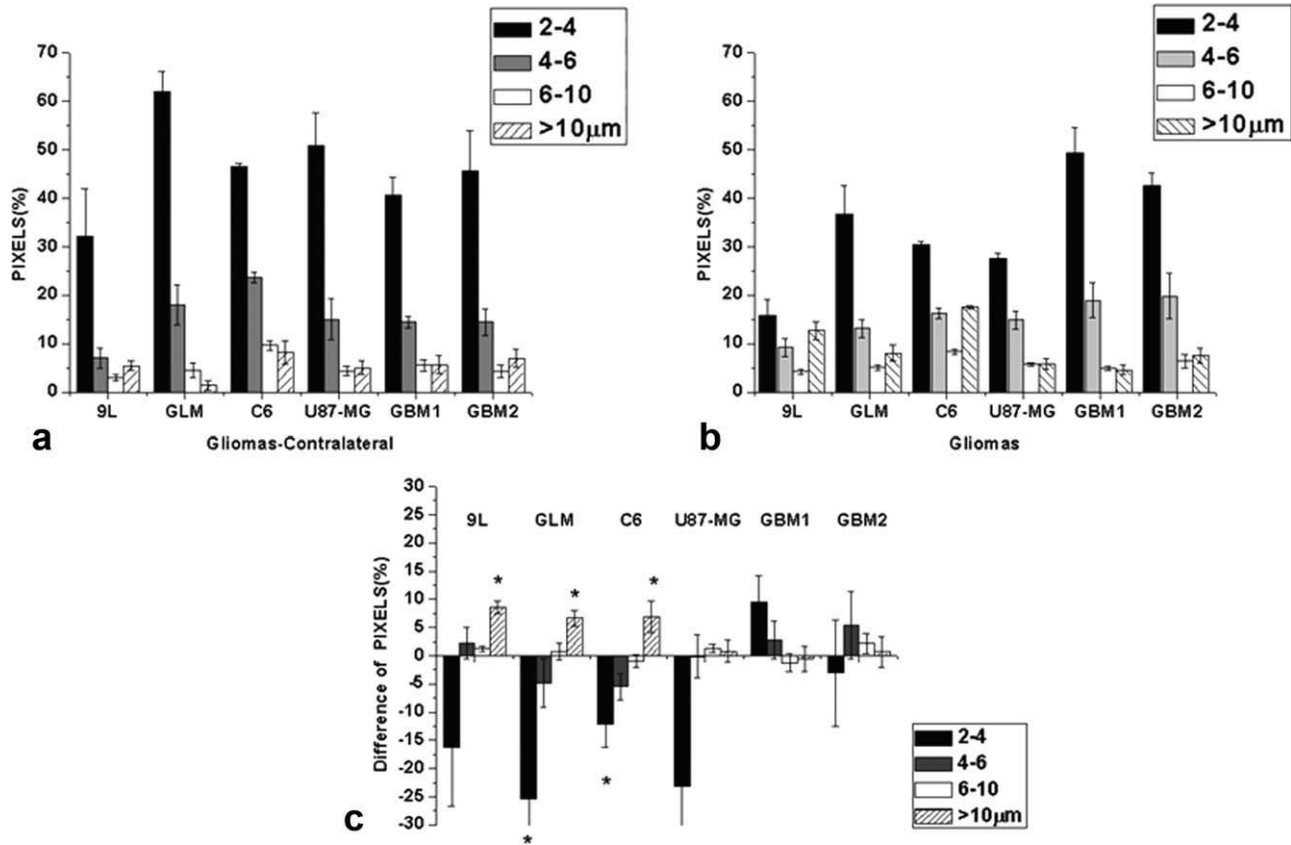


FIG. 5. Segmented VSI histograms. (A) VSI in the contralateral healthy part. (B) VSI in tumors. (C) Difference. VSI values over each tumor and its contralateral were divided into categories: 2–4  $\mu\text{m}$ , 4–6  $\mu\text{m}$ , 6–10  $\mu\text{m}$ , and over 10  $\mu\text{m}$ . \* indicates significant difference ( $P < 0.05$ ) using a paired t-test.

### Simple Histogram Analysis of VSI and BV

Tables 3 and 4 list  $P$ -values obtained after comparing each group of gliomas to their contralateral healthy part using several descriptive measures of the VSI and BV distributions. In both tables, significant  $P$ -values were highlighted. In the human gliomas, the statistical significance was not reached for all the descriptive parameters investigated.

In the gliomas of murine origin the 75th VSI percentile showed almost significant vessel caliber changes for C6 and 9L and a significant change for GLM gliomas. The shape of the GLM glioma VSI distribution showed also a significant change compared to the healthy part as seen from the skewness and kurtosis parameters describing the asymmetry and peakedness of the distributions, respectively. For the BV histogram analysis, the 25th percentile, median and 75th percentile of the C6 glioma  $\Delta R_2^*$  distributions were significantly different, whereas only the 75th percentile was significantly different for the GLM glioma BV distribution as well as the kurtosis parameter. The shape of the 9L glioma BV distribution also showed a significant variation. Apart from the C6 gliomas that demonstrated significant differences with GLM, GBM1, and GBM2 for the VSI mean, median and 75th percentile, the vascular distributions did not show significant differences between gliomas (Unpaired t-test  $P > 0.05$ ).

The differences in skewness and kurtosis for the GLM VSI histogram compared to their contralateral respective

histograms can readily be observed in Fig. 4A. The maximum vessel caliber of the healthy part of the GLM bearing rats was under 10  $\mu\text{m}$ , whereas the GLM vessel sizes increased over 30  $\mu\text{m}$ . 9L BV\* histograms evolved from a gaussian shape in the contralateral healthy brain into a broader distribution with a longer tail for the large BV values (Fig. 4B).

### Segmentation of Histograms

The distributions of vessel size indices in the healthy contralateral part of the rat brain were similar for all the rat strains (Fig. 5A). A large proportion of small vessels in the range 2–4  $\mu\text{m}$  was always represented (32%  $\pm$  19% for 9Lcontro, 39%  $\pm$  15% for C6contro, 41%  $\pm$  8.5% for GBM1contro, 45%  $\pm$  17% for GBM2contro and 62%  $\pm$  9% for GLMcontro) and smaller densities of pixels were found for the other categories of VSI with around 20% 4–6  $\mu\text{m}$  vessels and between 5 and 10% for 6–10  $\mu\text{m}$  and over 10  $\mu\text{m}$  vessels.

In the murine gliomas, a shift of VSI towards a higher density of vessels with bigger sizes was observed (Fig. 5B). Compared to the contralateral area, the number of tumor vessels with the lowest VSI was significantly lower (29%  $\pm$  3% vs 39%  $\pm$  15% for C6 [paired t-test,  $P = 0.0065$ ], 37%  $\pm$  13% vs 62%  $\pm$  9% for GLM [paired t-test,  $P = 0.03$ ]). However, the number of vessels in the category “over 10  $\mu\text{m}$ ” was significantly greater for GLM,

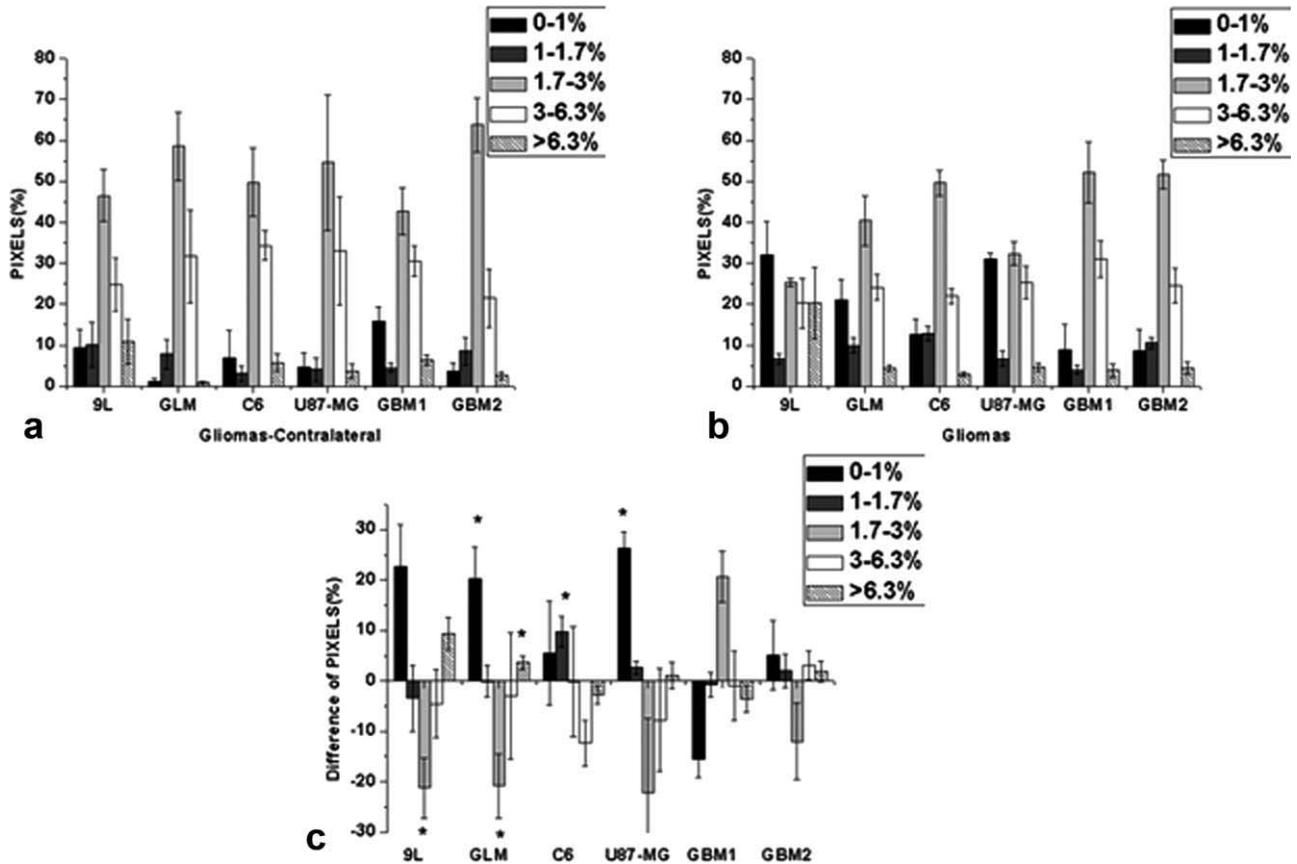


FIG. 6. Segmented BV histograms (A) BV in the contralateral healthy part. (B) BV in tumors (C) Difference. BV values over each tumor and its contralateral were divided into categories: 0.1, 1–1.7, 1.7–3, 3–6.3%, and over 6.3%. \* indicates significant difference ( $P < 0.05$ ) using a paired t-test.

C6 and 9L gliomas ( $8\% \pm 3.6\%$  vs  $1.4\% \pm 2.3\%$  for GLM [paired t-test  $P = 0.009$ ],  $20\% \pm 5\%$  vs  $10.4\% \pm 5.4\%$  for C6 [paired t-test  $P = 0.009$ ]).

In the gliomas of human origin, the distributions of VSI were similar to their contralateral part, both showing an important percentage of low VSI ( $48\% \pm 13\%$  in the GBM1 glioma and  $40.6\% \pm 8.5\%$  in the contralateral part;  $42.6\% \pm 5\%$  in the GBM2 glioma and  $45.7\% \pm 16.7\%$  in the contralateral part) and less than 10% VSI values over  $6 \mu\text{m}$ . GBM2 and GBM1 gliomas had also a larger proportion of low VSI values than the murine gliomas. The density of vessels of lower radius ( $2\text{--}6 \mu\text{m}$ ) was also higher in the GBM1 and GBM2 tumors than in the contralateral part of the brain. Figure 5C illustrates the difference between the VSI proportions in each glioma type and its contralateral part.

BV distributions over healthy parts of the rat brain were uniform (Fig. 6A). Their shapes were different for 9L and U87-MG gliomas. Pixels with BVs between 1.7 and 6.3% represented more than 70% of the total percentage of pixels encompassed in the ROI. The percentage of pixels with BVs in the same range were between 9% and 30% lower in all the gliomas except for GBM1 (Fig. 6B). The distribution of BV showed larger proportions of pixels with very low BV (0–1%) for all the gliomas except for GBM1, compared to their contralateral area ( $32\%$  vs  $9.4\%$  for 9L [Paired t-test,  $P = 0.07$ , not significant],  $21.1\%$  vs  $1.1\%$  in GLM [Paired t-test,  $P = 0.016$ ],  $8.8\%$  vs  $3.7\%$  in GBM2,  $8.9\%$  vs  $15.9\%$  in GBM1). C6, GBM1 and GBM2 showed differences in their

BV distributions compared to the 3 other gliomas. C6 demonstrated larger low BV proportions (0–1.7%) but smaller high BV proportions (3–>6.3%). The percentage of pixels with BV in the range 1.7–3% did not vary. For GBM2, all the BV categories of pixels showed larger proportions except for the pixels with BV between 1.7 and 3%. In contrast to all the other gliomas, GBM1 showed a larger percentage of pixels in the range 1.7–6.3% and a smaller percentage of pixels in the range 0–1%. Figure 6C illustrates the difference between BV proportions in each glioma type and its contralateral part.

The rats bearing GBM1 and GBM2 gliomas were imaged on two occasions. For GBM1 glioblastomas, the VSI distribution demonstrated a shift towards higher values with a higher number of pixels containing vessels of sizes above  $10 \mu\text{m}$  and a smaller number of pixels containing vessels of sizes under  $6 \mu\text{m}$ . In terms of BV, GBM1 demonstrated a larger number of pixels with lower BVs (0–1.7%) but a smaller number of pixels with higher BVs (1.7–>6.5%). For GBM2 gliomas, both the VSI and the BV distributions were conserved four days after the first MRI scan.

#### Vascular Architecture and Histology

Haematoxylin and eosin stained sections (not shown here) of 9L, C6 and GLM murine tumors revealed sharp delineation of the margins of tumors and little invasion of the contiguous normal brain for all the murine gliomas,

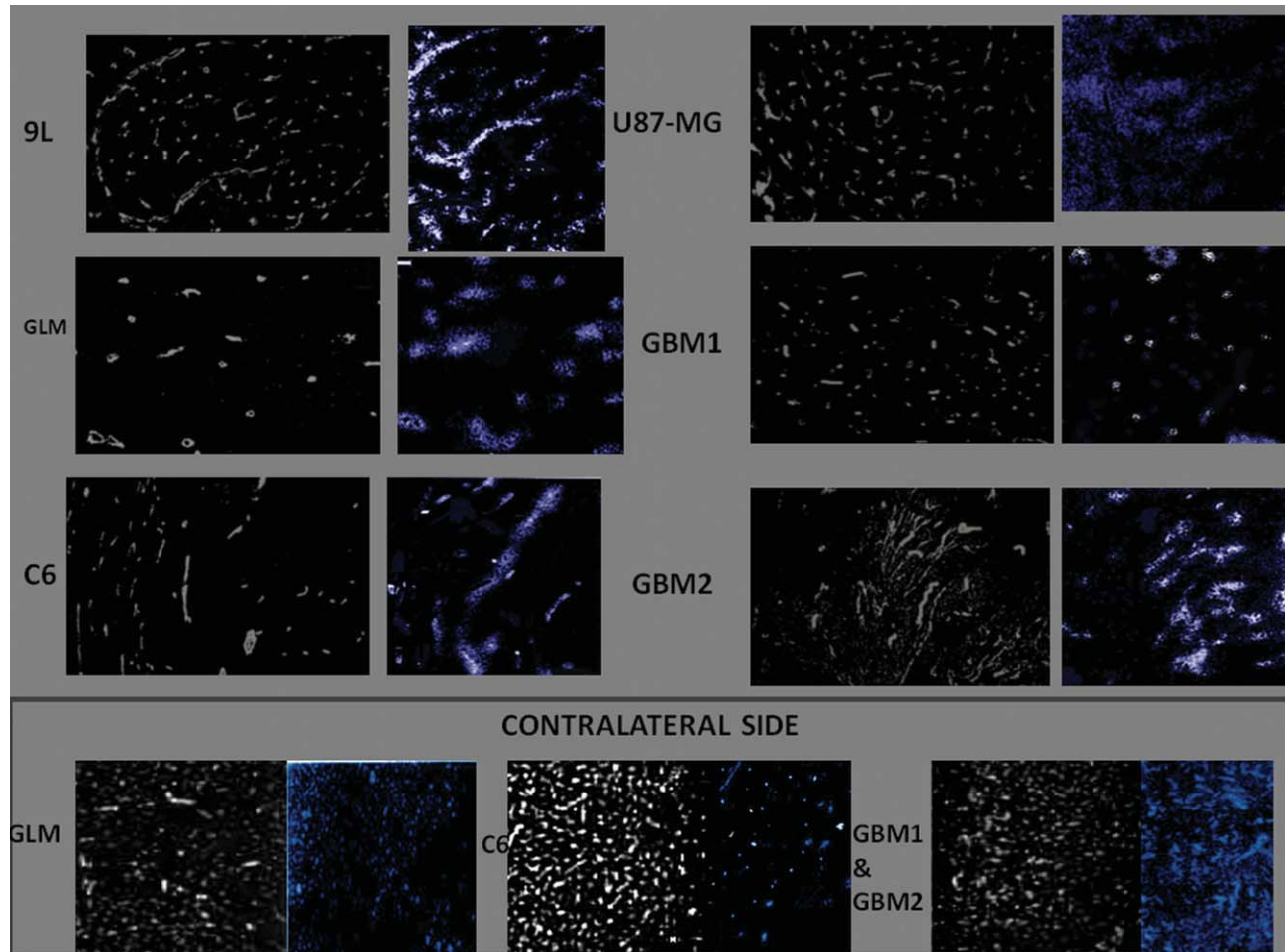


FIG. 7. Vascular architecture of intracerebral glioma xenografts of 9L, GLM, C6 and U87-MG, GBM1 and GBM2. Vessel structures are stained red with an antibody against the basal lamina component collagen IV using an immunofluorescence technique (Left images, magnification 200 $\times$ ). Normal brain vessels collagen IV stained sections are presented for contralateral side of GLM, C6 and GBM1 & 2. Figures illustrate the differences in vessel structure shape and size between the murine gliomas and the human gliomas and between normal brain vessels and brain tumor vessels. Blue stained Hoechst 33342 perfused vessels (Right images, Magnification 200 $\times$ ). Perfused blood vessels are delineated. Normal brain vessels Hoeschst stained are also presented for comparison purposes. [Color figure can be viewed in the online issue, which is available at [wileyonlinelibrary.com](http://wileyonlinelibrary.com).]

whereas human gliomas tended to show infiltration (GBM2) or undefined borders for GBM1 and U87-MG. C6 gliomas demonstrated characteristic foci of necrosis with pseudo-pallisading of tumor cells at the periphery. On the contrary, no or little necrosis was found in all the other gliomas. All the gliomas were characterized by strong cellular density compared to their contralateral side.

Immunohistochemical staining with collagen IV showed that all the murine gliomas demonstrated a lower density of vessels within tumors than in their contralateral healthy side (Fig. 7). In C6 gliomas, vessels were less numerous but larger and more elongated compared to 9L gliomas that showed a higher vascular density. In GLM gliomas, the vessels were sparsely distributed and widely separated from each other. All the murine gliomas presented enlarged vessel lumens compared to their contralateral part. Normal brain vessels appeared shorter and smaller and were also regularly arranged and numerous as shown in Fig. 7 for C6 and GLM.

Human gliomas demonstrated a similar vascular density to their contralateral side (GBM1 and GBM2 in Fig.

7). U87-MG tumors showed abundant vascular structures, which are homogeneously distributed. In GBM1, vessels were less numerous demonstrating small and short vessel structures. GBM2 tumors were composed of numerous elongated vessels oriented towards the periphery of tumors. GBM2 tumors demonstrated enlarged lumens, whereas in GBM1 and U87-MG tumors, the majority of vessels were similar to the contralateral side. Immunohistochemical staining with Hoechst 33342 (Fig. 7) showed that C6, GLM and GBM1 have a large proportion of functional and permeable vessels except for U87-MG and GBM2 that showed more permeable vessels than functional ones. In 9L gliomas, smaller vessels appeared to be less functional. A summary of the relevant VSI-MRI and histopathological results is given in Table 5.

## DISCUSSION

For an adequate development of antivascular and antiangiogenic treatment strategies, understanding the mechanisms of the markedly increased angiogenesis of high

Table 5  
Summary of VSI-MRI and Histopathological Data for Each Glioma Model

	Histopathology	VSI MRI
9L	Lower vascular density, enlarged vessel lumens Smaller radii vessels were less functional	High proportions of large vessels (>10 $\mu\text{m}$ ) Decreased proportions of BV (1.7–3%)
GLM	Sparsely distributed vessels, large inter-vascular distance Enlarged vessel lumens; High proportion of functional and permeable vessels	High proportions of large vessels (>10 $\mu\text{m}$ ); Low proportions of small radii vessels (2–6 $\mu\text{m}$ ) Decreased proportions of BV (1.7–3%); Increased proportions of BV >6.3%
C6	Lower vascular density, large elongated vessels Enlarged vessel lumens; Mostly functional and permeable vessels	High proportions of large vessels (> 10 $\mu\text{m}$ ); Low proportions of small radii vessels (2–6 $\mu\text{m}$ ) Increased proportions of BV (1–1.7%)
U87-MG	Abundant vascular structures, homogeneous distribution similar to contralateral No enlarged lumens/contralateral side; Mostly permeable vessels	No significant changes of vessel radii/contralateral side; decreased proportions of smaller Vessels (2–4 $\mu\text{m}$ ) relative to contralateral side; Increased proportions of small BV (0–1%)
GBM1	Vascular density identical to contralateral area Small and short vessel structures; no enlarged lumens/contralateral side Mostly functional and permeable	No significant changes of vessel radii/contralateral side; Increased proportions of smaller Vessels (2–6 $\mu\text{m}$ ) relative to contralateral side
GBM2	Vascular density identical to contralateral area, numerous Elongated vessels oriented towards the tumor periphery; enlarged lumens; Mostly permeable vessels	No significant BV difference with contralateral part No significant changes of vessel radii/contralateral side No significant BV difference with contralateral part

grade gliomas is crucial. Although a variety of brain tumors have been investigated in different rat strains, the available tumor models do not simulate human brain tumor growth and vascularization accurately. To optimize the imitation of the interaction of human gliomas with host endothelial cells, experimental glioma models must originate from glial cells and be implanted orthotopically to respect the characteristic glioma growth patterns: invasiveness, neovascularization and blood brain barrier alterations. The tumor growth must be of sufficient duration to allow therapeutic studies and the determination of treatment efficacy. Finally, immunological interferences must be minimized.

In the present study, the three human gliomas were all implanted orthotopically at an identical site in nude rats. Therefore, the differences in vascular parameters between U87-MG, GBM1 and GBM2 reflected angiogenic properties of the glioma cells derived from different primary human tumors. On the contrary, 9L, C6 and GLM tumors were implanted in different rat strains. There is growing evidence that interactions of the tumor cells and host cells are an important part of the complex process of glioma development (9). Hence, the vascular development of gliomas of murine origin most probably led to artificial growth patterns. Most studies in rat gliomas demonstrated rapid and well demarcated growth as opposed to slow and infiltrative growth patterns in human glioma models.

The vessel size MRI technique is based on a biophysical model describing the dephasing mechanisms that generate signal changes related to susceptibility changes induced by a contrast agent at the surface of vessels (5,10). The technique was designed to target changes in the total vasculature (from gradient echo data) and the

microvasculature (from spin-echo data) and to provide a measure of the mean vessel caliber. This description of the tumor vasculature showed its usefulness in many occasions (7,9,11,12). It demonstrated very good correlation with histological data and was therefore described as “a potentially noninvasive histological method”. For volume-matched tumors, the vascular parameters measured by MRI were clearly different between the gliomas of murine origin and the gliomas of human origin. Marked increased vessel sizes were measured in all the three murine brain tumors whereas the three human gliomas had similar vessel sizes to their contralateral healthy brain part both using ROI and histogram analyses.

In most cancer studies, quantitative analysis is commonly performed using multiple small-region of interest (ROI) measurements from which mean and/or median values are often compared. Most malignant gliomas are characterized by their high heterogeneity. Their vasculature can be significantly different from one small ROI to another due to vessel dilation, important necrosis, high vessel tortuosity, permeability and changes in functionality (13). Upon treatment, these different regions may have different responses and powerful techniques are needed to discriminate between them. Histogram analysis allows the analysis of distributions of pixels over tumors. Specific areas can therefore be analyzed against others (14). In the present work, only murine gliomas showed significant differences in percentiles compared to their healthy contralateral part.

In a recent study (15), the VSI MRI technique was combined with histogram analysis to follow the effects of an antivascular treatment in a rodent tumor model. The 25th percentiles of BV and VSI were significantly more sensitive to antivascular treatment than median

values, which could be interpreted as a sign of vascular collapse of bigger vessels.

Here, with histogram segmentation, specific vascular differences were identified: all the murine gliomas showed higher proportions of vessels with increased calibers and simultaneously smaller proportions of vessels with the lowest calibers and thus suggest a dilation of the already existing vessels but no generation of new vessels. GBM1 and GBM2 glioblastomas demonstrated no significant evolution of the numbers of vessels in all the categories of vessels. A tendency towards higher percentages of vessels with the lowest vessel calibers were found in GBM1. No significant evolution of the numbers of vessels above 10  $\mu\text{m}$  was noticed. These results suggest that new vessels were potentially developed in GBM1.

The mean VSI value was  $6.54 \pm 0.6 \mu\text{m}$  in our C6 tumors. Using multiple small ROI analysis, Tropres et al. (7) and others (9,16,17) reported mean VSI values between  $4.1 \pm 2.1 \mu\text{m}$  and  $5.8 \pm 4.1 \mu\text{m}$  in C6 tumors. In the present work, C6 tumor mean BVs (2.8%) were lower compared to the contralateral healthy side (3.5%). Tropres et al. (7) also showed that in viable C6 tumor tissue, the BV was lower ( $2\% \pm 0.7\%$ ) than in the contralateral cortical area ( $4.3\% \pm 0.3\%$ ). The reasons for a decrease of BV values in C6 gliomas were attributed to the lower vessel density found in C6 tumors compared to their contralateral part but other hypotheses mentioned abnormal tumor development with vessel co-option followed by possible degeneration or regression (18). 9L BVs were greater (3.5%) compared to the contralateral healthy side (2.6%) and Pathak et al. (9) also found larger BV in 9L gliosarcomas implanted in Fisher rats compared to the normal brain. In the contralateral healthy brain, the total vascular BVs in the range 1.7–6.5% represented between 70 and 90% of the BVs. This range of BVs was noticeably smaller in all the gliomas except for GBM1. These differences seemed compensated by larger BVs below 1% and suggested the development of new blood vessels. The segmented histogram analysis showed that depending on the tumor line considered, BVs were distributed differently: in C6 tumors, BVs up to 1.7% represented around 25% of the total averaged BVs, whereas this range of BVs represented only 8% of the total averaged BVs in normal tissue. In 9L tumors, the percentage of pixels with BVs below 1% reached 30% against 10% in normal tissue. Simultaneously, 20% of the tumor pixels represented BVs over 6.5% against 10% in normal tissue.

Depending on the murine glioma cell type, antiangiogenic treatments such as vascular endothelial growth-receptor tyrosine kinase inhibitors demonstrated either no effects (19) or partial suppression of larger vessels (20,21) and similarly either no effects on the growth of new smaller-diameter vessels (20,21) or reduced occurrence of microvessels at the center of the tumor mass (19). The response to antiangiogenic agents of murine gliomas was different from the response of human glioma. The segmentation of histograms of vessel size indices could be a good noninvasive indicator for making decisions regarding treatment doses or combinations of treatment to target small vessels or established vessels or even for treatment

timing during tumor growth. For the analysis of VSI data in gliomas, histogram analysis could be a more appropriate method to target vascular changes upon antiangiogenic or antivascular treatment and could even help decisions regarding treatment dosage, timing and combination since specific vessel sizes and BVs can be assessed.

As mentioned by Pathak et al. (9), the common practice to determine if MRI BV methods are appropriate markers of angiogenesis is to compare BV measurements to histological measurements of microvessel density (MVD). However, good correlations between areas of intense neovascularization were not always obtained (8,22). In the present case, VSI and BV values represent weighted averages over these pixels. Thus, one pixel may contain a single large caliber vessel representing a low BV, whereas another pixel may contain several small caliber vessels that will represent on average a small caliber vessel but a high BV. Displaying histogram distributions of vascular parameters may help to resolve inconsistencies between MR methods and histological methods. Higher spatial resolutions may also improve the power of histogram analysis.

Immunohistochemical findings were in agreement with MRI findings although only a qualitative analysis was performed. To qualify and validate the different angiogenic phenotype inferred from the MRI data, correlations with quantitative immunohistochemical data as in (8) will be needed in the future. However, there is already an abundant literature reporting quantitative parameters such as vascular density and perfusion parameters derived from immunohistochemical staining in C6, 9L (9,23,24) and human glioblastomas (13). Most studies demonstrated strong correlations between quantitative VSI MRI parameters and histopathological data (7,9,25–27) in various tumor types. Therefore, we are confident that quantitative histology should confirm the VSI and BV findings of the present study. However, reports from one study to another may be contradictory. BV determined with susceptibility MRI already demonstrated to correlate with Hoechst 33342 uptake (28) but this result cannot be assumed for all the tumors. In the present study and in (9), 9L gliosarcomas presented higher mean and median BV than their contralateral part while Hoechst staining of 9L showed that not all the smaller vessels were perfused. Other immunohistochemical staining studies (23,24) showed that 9L tumors were less perfused with a smaller vascular density relative to their contralateral part suggesting a lower BV. A potential answer to these differences may be given by the segmented histogram analysis showing that only the 0–1% and over 6% BV categories were increased relative to the contralateral side in 9L. This analysis technique may therefore be helpful to reveal the heterogeneous perfusion effects in tumors. Although only qualitative, immunohistochemical findings provided a visualization of the vessel sizes (diameter and length) and an evaluation of the distribution of vessels within the different gliomas and their contralateral side. Descriptions of the tumors vascular morphology and spatial heterogeneity were in agreement with the MRI data.

One current limitation of the VSI MRI technique is that it does not account for vessel tortuosity frequently related

to malignancy by histological examination (29). Tortuous vessels in tumors can be capillaries or larger vessels before vessel sprouting (29). Vessel calibers and BV may therefore differ from one slice to another or only parts of vessels may be mapped, which may impact on BV estimates. Vessel tortuosities also affect blood flows and mean transit times (MTTs) and therefore affect the functionality of tumor vessels. The tumor perfusion may therefore show considerable variation between tumors derived from the same tumor line and between tumor lines (13). It may be useful in the future to perform tumor blood flow measurements in combination with VSI MRI and correlate these measurements using histogram analysis.

## CONCLUSION

A pixel-by-pixel analysis was performed to produce histogram distributions and parametric maps of VSI and BVs in each glioma. The frequency distributions of VSI and BV showed that vascular distributions are different in gliomas of murine origin and in gliomas of human origin. The further segmentation of histograms into categories of VSI and BV and the analysis of the correlation between VSI and BV suggest that histogram analysis may provide specific information about tumor vascularization, microvascular morphology and spatial heterogeneity in agreement with qualitative immunohistochemical findings and help improve treatment strategies. In addition, these results suggest these methods of analysis should be included in further similar studies to provide information on the tumor angiogenic phenotype.

## REFERENCES

- Li KL, Wimes LJ, Henry RG, Pallavicini MG, Park JW, Hu-Lowe DD, McShane TM, Shalinsky DR, Fu YJ, Brasch RC, Hylton NM. Heterogeneity in the angiogenic response of a BT474 human breast cancer to a novel vascular endothelial growth factor-receptor tyrosine kinase inhibitor: assessment by voxel analysis of dynamic contrast enhanced MRI. *J Magn Reson Imaging* 2005;22:511–519.
- Emblem KE, Nedregaard B, Nome T, Due-Tonnessen P, Hald JK, Scheie D, Borota OC, Cvanarova M, Bjornerud A. Glioma grading by using histogram analysis of blood volume heterogeneity from MR derived cerebral blood volume maps. *Radiology* 2008;247:808–817.
- Bogler O, Mikkelsen TA. Angiogenesis in glioma: molecular mechanisms and roadblocks to translation. *Cancer J* 2003;9:205–213.
- Anderson JC, McFarland BC, Gladson CL. New molecular targets in angiogenic vessels of glioblastoma tumours. *Exp Rev Mol Med* 2008;10:1–26.
- Tropres I, Grimault S, Vaeth A, Grillon E, Julien C, Payen JF, Lamalle L, Décorps M. Vessel size imaging. *Magn Reson Med* 2001;45:397–408.
- Kiselev VG, Strecker R, Ziyeh S, Speck O, Hennig J. Vessel size imaging in humans. *Magn Reson Med* 2005;53:553–563.
- Tropres I, Lamalle L, Peoc'h M. In vivo assessment of al angiogenesis. *Magn Reson Med* 2004, 51:533–541.
- Robinson SP, Rijken PF, Howe FA, McSheehy PM, van der Sanden BP, Heerschap A, Stubbs M, van der Kogel AJ, Griffiths JR. Tumor vascular architecture and function evaluated by non-invasive susceptibility MRI methods and immunohistochemistry. *J Magn Reson Imaging* 2003;17:445–454.
- Pathak AP, Schmainda KM, Ward BD, Linderman JR, Rebro KJ, Greene AS. MR-derived cerebral blood volume maps: issues regarding histological validation and assessment of angiogenesis. *Magn Reson Med* 2001;46:735–747.
- Jensen JH, Chandra R. MR imaging of microvasculature. *Magn Reson Med* 2000;44:224–230.
- Ferretti S, Allegrini PR, O'Reilly T, Schnell C, Stumm M, Wartmann M, Wood J, McSheehy PM. Patupilone induced vascular disruption in orthotopic rodent models detected by magnetic resonance imaging and interstitial fluid pressure. *Clin Cancer Res* 2005;11:7773–7784.
- Wade TP, Kozlowski P. Longitudinal studies of angiogenesis in hormone-dependent Shionogi tumours. *Neoplasia* 2007;9:563–568.
- Bernsen HJJA, Rijken PFJW, Hagemeier NE, van der Kogel AJ. A quantitative analysis of vascularization and perfusion of human glioma xenografts at different implantation sites. *Microvasc Res* 1999, 57:244–257.
- Young R, Babb J, Law M, Pollack E, Johnson G. Comparison of region-of-interest analysis with three different histogram analysis methods in the determination of perfusion metrics in patients with brain gliomas. *J Magn Reson Imaging* 2007;26:1053–1063.
- Howe FA, McPhail LD, Griffiths JR, McIntyre DJ, Robinson SP. Vessel size index magnetic resonance imaging to monitor the effect of antivascular treatment in a rodent model. *Int J Radiat Oncol Biol Phys* 2008;71:1470–1476.
- Dennie J, Mandeville JB, Boxerman JL, Packard SD, Rosen BR, Weisskoff RM. NMR imaging of changes in vascular morphology due to tumor angiogenesis. *Magn Reson Med*. 1998;40:793–799.
- Farell CL, Farell CR, Stewart PA, Del Maestro RF, Ellis CG. The functional microcirculation in a glioma model. *Int J Radiat Biol* 1991;60: 131–137.
- Holash J, Maisonpierre PC, Compton D, Boland P, Alexander CR, Zagzag D, Yancopoulos GD, Wiegand SJ. Vessel cooption, regression and growth in tumours mediated by angiopoietins and VEGF. *Science* 1999;284:1994–1998.
- Wood JM, Bold G, Buchdunger E, Cozens R, Ferrari S, Frei J, Hofmann F, Mestan J, Mett H, O'Reilly T, Persohn E, Rösel J, Schnell C, Stover D, Theuer A, Towbin H, Wenger F, Woods-Cook K, Menrad A, Siemeister G, Schirner M, Thierauch KH, Schneider MR, Drevs J, Martiny-Baron G, Totzke F. PTK787/ZK 222584, a novel and potent inhibitor of vascular endothelial growth factor-induced responses and growth after oral administration. *Cancer Res* 2000;60:2178–2189.
- Quarles CC, Schmainda KM. Assessment of the morphological and functional effects of the anti-angiogenic agent SU11657 on 9L gliosarcoma vasculature using dynamic susceptibility contrast MRI. *Magn Reson Med* 2007;57:680–687.
- Mendel DB, Laird AD, Xin X, Louie SG, Christensen JG, Li G, Schreck RE, Abrams TJ, Ngai TJ, Lee LB, Murray LJ, Carver J, Chan E, Moss KG, Haznedar JO, Sukbunthorn J, Blake RA, Sun L, Tang C, Miller T, Shirazian S, McMahon G, Cherrington JM. In vivo antitumor activity of SU11248, a novel tyrosine kinase inhibitor targeting vascular endothelial growth factor and platelet-derived growth factor receptors: determination of pharmacokinetic/pharmacodynamic relationship. *Clin Cancer Res* 2003;9:327–337.
- Kostourou V, Robinson SP, Whitley GS, Griffiths JR. Effects of over-expression of dimethylarginine dimethylaminohydrolase on tumor angiogenesis assessed by susceptibility magnetic resonance imaging. *Cancer Res* 2003;63:4960–4966.
- Chertok B, David AE, Huang Y, Yang VC. Glioma selectivity of magnetically targeted nanoparticles: a role of abnormal tumor hydrodynamics. *J Control Release* 2007;122:315–323.
- Arosarena O, Guerin C, Brem H, Laterra J. Endothelial differentiation in intracerebral and subcutaneous experimental gliomas. *Brain Res* 1994;640:98–104.
- Valable S, Lemasson B, Farion R, Beaumont M, Segebarth C, Remy C, Barbier EL. Assessment of blood volume, vessel size, and the expression of angiogenic factors in two rat glioma models: a longitudinal in vivo and ex vivo study. *NMR Biomed* 2008;21: 1043–1056.
- Douma K, Oostendorp M, Slaaf DW, Post MJ, Backes WH, van Zandvoort MA. Evaluation of magnetic resonance vessel size imaging by two-photon laser scanning microscopy. *Magn Reson Med*. 2010;63: 930–939.
- Ungersma SE, Pacheco G, Ho C, Yee SF, Ross J, van Bruggen N, Peale FV Jr, Ross S, Carano RA. Vessel imaging with viable tumor analysis for quantification of tumor angiogenesis. *Magn Reson Med* 2010;63: 1637–1647.
- Robinson SP, Howe FA, Griffiths JR, Ryan AJ, Waterton JC. Susceptibility contrast magnetic resonance imaging determination of fractional tumor blood volume: a noninvasive imaging biomarker of response to the vascular disrupting agent ZD6126. *Int J Radiat Oncol Biol Phys* 2007;69:872–879.
- Bullitt E, Ewend MG, Aylward S, Lin W, Gerig G, Joshi S, Jung I, Muller K, Smith JK. Abnormal vessel tortuosity as a marker of treatment response of malignant gliomas: preliminary report. *Technol Cancer Res Treat* 2004;3:577–584